Monolithically integrated all-optical gate switch using intersubband transition in InGaAs/AlAsSb coupled double quantum wells

Ryoichi Akimoto,* Shin-ichiro Gozu, Teruo Mozume, and Hiroshi Ishikawa

Network Photonics Research Center, National Institute of Advanced Industrial Science and Technology (AIST), AIST Tsukuba central 2-1, 1-1-1 Umezono, Tsukuba, Ibaraki 305-8568, Japan
**r-akimoto@aist.go.jp*

Abstract: We have developed a compact all-optical gate switch with a footprint less than 1 mm^2, in which an optical nonlinear waveguide using cross-phase-modulation associated with intersubband transition in InGaAs/AlGaAs/AlAsSb coupled double quantum wells and a Michelson interferometer (MI) are monolithically integrated on an InP chip. The MI configuration allows a transverse magnetic pump light direct access to an MI arm for phase modulation while passive photonic integrated circuits serve a transverse electric signal light. Full switching of the π-rad nonlinear phase shift is achieved with a pump pulse energy of 8.6 pJ at a 10-GHz repetition rate. We also demonstrate all-optical demultiplexing of a 160-Gb/s signal to a 40-Gb/s signal.

OCIS codes: (190.5970) Semiconductor nonlinear optics including MQW; (130.4815) Optical switching devices.

References and links

1. H. Ishikawa, *Ultrafast All-Optical Signal Processing Devices*, (Wiley, 2008) Chap. 5.
2. H. Tsuchida, T. Simoyama, H. Ishikawa, T. Mozume, M. Nagase, and J. Kasai, "Cross-phase-modulation-based wavelength conversion using intersubband transition in InGaAs/AlAs/AlAsSb coupled quantum wells," Opt. Lett. **32**(7), 751–753 (2007).
3. H. Ishikawa, H. Tsuchida, K. S. Abedin, T. Simoyama, T. Mozume, M. Nagase, R. Akimoto, T. Miyazaki, and T. Hasama, "Ultrafast all-optical refractive index modulation in intersubband transition switch using InGaAs/AlAs/AlAsSb quantum wells," Jpn. J. Appl. Phys. **46**(8), L157–L160 (2007).
4. G. W. Cong, R. Akimoto, M. Nagase, T. Mozume, T. Hasama, and H. Ishikawa, "Mechanism of ultrafast modulation of the refraction index in photoexcited $In_xGa_{1-x}As/AlAs_ySb_{1-y}$ quantum well waveguides," Phys. Rev. B **78**(7), 075308 (2008).
5. G. W. Cong, R. Akimoto, K. Akita, S. Gozu, T. Mozume, T. Hasama, and H. Ishikawa, "Experimental and theoretical study of cross phase modulation in InGaAs/AlAsSb coupled double quantum wells with AlGaAs coupling barrier," Phys. Rev. B **80**(3), 035306 (2009).
6. S. Gozu, T. Mozume, R. Akimoto, I. Akita, C. Guangwei, and H. Ishikawa, "Cross Phase Modulation Efficiency Enhancement in In0.8Ga0.2As /Al0.5Ga0.5As/ AlAs0.56Sb0.44 Coupled Double Quantum Wells by Tailoring Interband Transition Wavelength," Appl. Phys. Express **2**, 42201 (2009).
7. R. Akimoto, T. Simoyama, H. Tsuchida, S. Namiki, C. G. Lim, M. Nagase, T. Mozume, T. Hasama, and H. Ishikawa, "All-optical demultiplexing of 160- to 10-Gb/s signals with Mach-Zehnder interferometric switch utilizing intersubband transition in InGaAs/AlAs/AlAsSb quantum well," Appl. Phys. Lett. **91**(22), 221115 (2007).
8. R. Akimoto, G. W. Cong, T. Mozume, S. Gozu, H. Tsuchida, T. Hasama, and H. Ishikawa, ""All-Optical Demultiplexing from 160 to 40/80 Gb/s Using Mach-Zehnder Switches based on Intersubband Transition of InGaAs/AlAsSb Coupled Double Quantum Wells," IEICE ELECTRON," E **92-C**, 187–192 (2009).
9. R. Akimoto, S. Gozu, T. Mozume, K. Akita, G. W. Cong, T. Hasama, and H. Ishikawa, "All-Optical Wavelength Conversion at 160Gb/s by Intersubband Transition Switches Utilizing Efficient XPM in InGaAs/AlAsSb Coupled Double Quantum Well," in *Proceedings of 35th European Conference on Optical Communication*, (VDE VERLAG GMBH, Berlin, 2009)1.2.2.
10. T. Kurosu, S. Namiki, R. Akimoto, H. Kuwatsuka, S. Sekiguchi, N. Yasuoka, K. Morito, H. Hasama, and H. Ishikawa, "Demonstration of 172-Gb/s Optical Time Domain Multiplexing and Demultiplexing Using Integratable Semiconductor Devices," IEEE Photon. Technol. Lett. **22**(19), 1416–1418 (2010).
11. G. W. Cong, R. Akimoto, S. Gozu, T. Mozume, T. Hasama, and H. Ishikawa, "Simultaneous generation of intersubband absorption and quantum well intermixing through silicon ion implantation in undoped InGaAs/AlAsSb coupled double quantum wells," Appl. Phys. Lett. **96**(10), 101901 (2010).

#143905 - $15.00 USD Received 24 Mar 2011; revised 19 May 2011; accepted 1 Jun 2011; published 27 Jun 2011

12. G. W. Cong, R. Akimoto, S. Gozu, T. Mozume, T. Hasama, and H. Ishikawa, "All-optical Cross-phase Modulation Generation by Ion Implantation in III-V Quantum Wells," IEEE Photon. Technol. Lett. **22**(24), 1820–1822 (2010).
13. R. Schnabel, W. Pieper, A. Ehrhardt, M. Eiselt, and H. G. Weber, "Wavelength conversion and switching of high speed data signals using semiconductor laser amplifiers," Electron. Lett. **29**, 2047 (1993).
14. B. Mikkelsen, M. Vaa, H. N. Poulsen, S. L. Danielsen, C. Joergensen, A. Kloch, P. B. Hansen, K. E. Stubkjaer, K. Wunstel, K. Daub, E. Lach, G. Laube, W. Idler, M. Schilling, and S. Bouchoule, "40Gbit/s all-optical wavelength converter and RZ-to-NRZ format adapter realised by monolithic integrated active Michelson interferometer," Electron. Lett. **33**(2), 133–134 (1997).

1. Introduction

Ultrafast all-optical phase modulation is a key component for high-speed signal processing such as in all-optical demultiplexing and wavelength conversion of high-bit-rate (above 100-Gbit/s) optical time-division-multiplexed (OTDM) signals. Currently, such high-speed all-optical devices based on optical nonlinearity in fibers and semiconductor optical amplifiers (SOAs) are under intense investigation. The latter have advantages such as the possibility of device miniaturization, high stability, and low switching power. However, a pattern effect caused by slow carrier relaxation inherent to interband transition is regarded as a potential issue during high-speed operation. Intersubband transitions (ISBTs) in semiconductor quantum wells (QWs) have an advantage in this respect, as a typical ISBT carrier relaxation time in a QW is sub-ps to a few ps, making it free from the pattern effect beyond 100-Gb/s operation [1]. In particular, in InGaAs/AlAs/AlAsSb coupled double QWs (CDQWs), a novel modulation mechanism associated with ISBT has been found in which transverse electric (TE) light immune to ISBT absorption is phase-modulated by ISBT excitation due to transverse magnetic (TM) light [2,3]. This cross-phase modulation (XPM) has a unique polarization feature in that TE light does not suffer from a large insertion loss due to the ISBT absorption. XPM has been found to originate from modulation of an interband dispersion by intersubband excitation [4,5]. That is, when electrons at the first conduction subband are pumped to upper conduction subbands, the interband absorptions and refractive indices corresponding to the optical transitions between the valence subbands and the first conduction subband are changed because of depression of the electron population at the first subband. Therefore, the XPM response time is determined by fast electron relaxation from the upper subbands to the first subband. In accord with this mechanism, XPM efficiency has been improved to 0.5 rad/pJ using InGaAs /AlAsSb CDQWs with a AlGaAs coupling barrier [6].

A Mach-Zehnder interferometer (MZI) gate switch using the XPM effect associated with ISBT has been developed [7]. Using this device, all-optical signal processing experiments such as demultiplexing from 160 to 40 Gb/s [8], wavelength conversion at 160 Gb/s [9], and NRZ-RZ conversion at 40 GHz [10] have been demonstrated. However, the MZI gate switch used in these cases is constructed by bulk optic components in a free-space layout, in which an ISBT waveguide chip for XPM is placed in one MZI arm. This results in a large module size with a footprint on the order of ~10^2 cm^2 and mechanical instability of interferometric conditions due to environmental changes. This gate switch is unsuitable for large-scale integration, in which many all-optical gate switches are placed on a chip to realize parallel signal processing for high-capacity data rates. Therefore, a compact and monolithically integrated device in a single chip is highly desired. A challenge for monolithic integration is to realize ISBT and non-ISBT waveguides on a planar chip for XPM and light propagation, respectively, in an area-selective manner. One approach to achieve monolithic integration is selective-area activation of ISBT absorption by Si-ion implantation into undoped CDQWs [11]. However, this method remains challenging because the XPM efficiency is less than 0.1 rad/pJ [12]. Another approach is to use the Michelson interferometer (MI) configuration, which can be viewed as a folded version of the MZI configuration. One benefit of an MI-based all-optical gate switch is that a pump light can gain direct access to the phase modulation component in an MI arm through a reflective facet. This concept was first implemented in an all-optical wavelength converter using XPM in an SOA chip with a reflective facet on one side placed at one arm of a fiber-based MI [13]. Later, a monolithically integrated version was realized [14].

#143905 - $15.00 USD Received 24 Mar 2011; revised 19 May 2011; accepted 1 Jun 2011; published 27 Jun 2011

In this paper, we demonstrate for the first time a compact and monolithically integrated ultrafast all-optical gate switch based on ISBT with a footprint of less than 1 mm^2 using the MI configuration. In this gate switch, one of the arms in the MI functions as a nonlinear waveguide using a reflective XPM effect. Full switching of the π-rad nonlinear phase shift is confirmed at a 10-GHz repetition rate. In addition, we demonstrate all-optical demultiplexing of a 160-Gb/s signal to a 40-Gb/s signal.

2. Design and fabrication

A schematic diagram of the monolithically integrated all-optical gate switch and a photo of the device undergoing testing are shown in Fig. 1. The 1-mm-long device based on an MI consists of a 3-dB multi mode interference (MMI) coupler. The MI is designed to work for TE light. The waveguide is 1.6 μm wide except for the input/output ports, where the waveguide width is gradually increased to 2.5 μm for better optical coupling with a lensed fiber. The facet on the right is anti-reflection (AR) coated for the input/output of the TE signal, whereas that on the left is half-reflection (HR) coated at R = 50% for TE signal reflection, so that the two arms on the left of the MMI coupler function as the MI arms for interference. Given that one of the ports on the left is also used for the TM pump input, the reflectivity of HR is determined by the tradeoff between TM pump coupling and TE signal reflection.

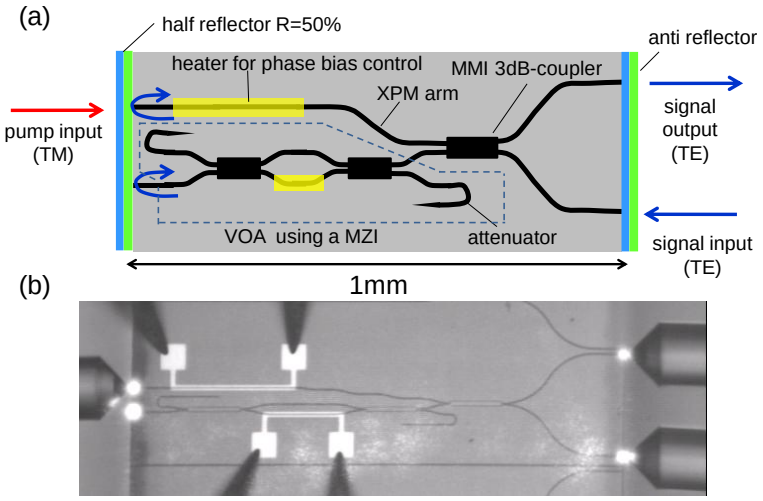

Fig. 1. (a) Schematic of the monolithically integrated all-optical gate switch based on a Michelson interferometer. VOA: variable optical attenuator; MZI: Mach-Zehnder interferometer; MMI: multi-mode interference; XPM: cross-phase modulation. (b) Microscope image of the fabricated chip undergoing a test taken by infrared camera. Bright spots at input/output ports are scattered light at facets when a TE signal light at 1560 nm is launched from the signal input port.

One of the MI arms functions as a nonlinear waveguide (the XPM arm) when a TM pump is launched into the XPM arm, i.e., a nonlinear phase shift occurs in a TE signal light that propagates in the waveguide region where the TM pump is absorbed. Therefore, the ISBT absorption magnitude is adjusted by Si-doping conditions during the epitaxial growth of a wafer so that the TM pump attenuates completely in the XPM arm. A resistive heater is attached to the XPM arm to control a static phase bias between the two arms in the MI. On the other MI arm, a variable optical attenuator (VOA) is formed to maintain a power balance between the two MI arms. This is because a signal loss occurs in the XPM arm due to a thermal red shift of the interband absorption edge in the case of high pump power injection. VOA function is achieved by an MZI with a heater for controlling light attenuation. As for the two ports connected to the MZI, a U-shaped waveguide with a bending radius of 10 μm and

#143905 - $15.00 USD Received 24 Mar 2011; revised 19 May 2011; accepted 1 Jun 2011; published 27 Jun 2011

an inverse taper with a tip width of 0.3 μm are attached to attenuate signals directed to these ports completely during VOA operation.

The wafer for the device was grown on a semi-insulating InP substrate by the molecular beam epitaxy method. After the growth of an InP buffer, a 0.55-μm-thick waveguide core composed of a separate confinement hetero (SCH) structure was grown. The SCH structure consists of a 0.2-μm-thick intersubband active layer of InGaAs/AlGaAs/AlAsSb CDQWs [5], which is sandwiched by optical guiding layers of 0.175-μm-thick InGaAs/AlAsSb multiple quantum wells (MQWs). The InGaAs well layers in CDQWs are Si-doped to activate intersubband absorption. After growing the layers for SCH, a 1-μm-thick InP upper cladding layer was grown.

A photonic integrated circuit pattern was defined by electron beam lithography. A composite etching mask composed of 0.3-um-thick SiO_2 and Ti/Ni (10/45 nm-thick) was formed by the metal deposition/lift-off technique and subsequent reactive ion etching of the SiO_2 layer deposited on the as-grown wafer. A deep-etched mesa waveguide with a depth of 2.0 μm was fabricated by inductively coupled plasma (ICP) dry etching using a mixture of Ar and BCl_3 gases. After ICP etching, the composite mask was removed by a buffered hydrofluoric acid. The etched surface was passivated by a 50-nm-thick Si_3N_4 layer, and planarized by a polymer of benzocyclobutene (BCB) to protect the mesa for later fabrication processes. The Ti/Au heater (10/100 nm-thick, 10-μm-wide) was formed on the surface planarized by the BCB polymer. A cleaved facet for the TE signal input/output was AR-coated by a double layer of dielectric materials (SiO_2 and ZrO_2), whereas the opposite facet for the pump input as well as signal reflection was HR-coated using the same materials.

3. Experimental results and discussions

3.1 Waveguides properties

The transmission property in a straight waveguide is examined to identify intersubband and interband transitions in the present CDQWs. Figure 2(a) shows the spectra of fiber-to-fiber transmittance in a 250-μm-long straight waveguide with both facets AR-coated. The TM spectra show that a broad absorption band centered at ~1500nm due to ISBT (e1-e4) covers the entire C-band spectral range (λ = 1.54–1.56 μm) with an absorption loss of ~40 dB/mm at 1550 nm. On the shorter wavelength side of ISBT band, the interband absorption (e1-light hole1) appears from ~1430 nm. On the other hand, the TE spectrum shows that an interband absorption (e1-heavy hole1) edge locates at ~1520 nm, and the waveguide is transparent to TE light in the spectral range longer than this wavelength. Subband energy levels in conduction and valence bands in the CDQW are shown in Fig. 2 (b).

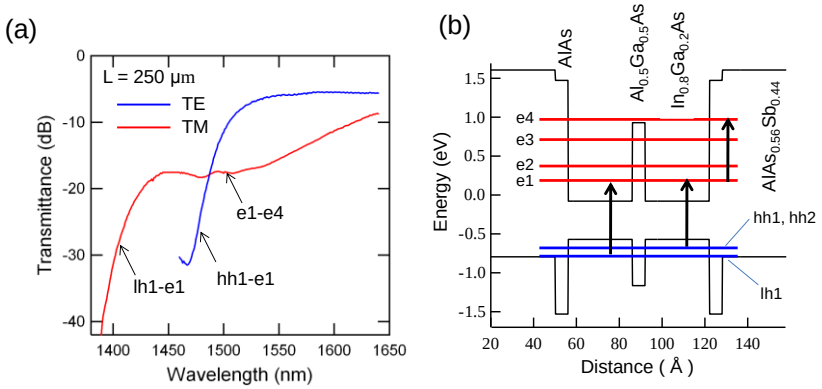

Fig. 2. (a) Fiber-to-fiber transmittance for TE and TM polarization in a 250-μm-long straight waveguide, fabricated from the same wafer of the all-optical gate switch. The transmittance includes coupling losses between fiber and waveguide. (b) Band diagram in CDQW. Energy levels of e1 to e4 denote subbands in a conduction band, whereas hh and lh denote heavy-hole

#143905 - $15.00 USD Received 24 Mar 2011; revised 19 May 2011; accepted 1 Jun 2011; published 27 Jun 2011

and light-hole subbands in a valence band, respectively. The vertical allows indicate the optical transitions shown in (a).

The XPM effect of a 1-mm-long straight waveguide is examined in different combinations in light propagation direction of the TM pump and TE probe. In the present all-optical gate switch, it is necessary that the probe light be reflected at the end of the XPM arms. Therefore, the XPM effect in the probe light accumulates in two situations, i.e., counter-propagation of pump and probe before a facet reflection and co-propagation after a facet reflection. This is different from the MZI-based gate switch in which the pump and probe always propagate in the same direction. Figure 3(a) shows a schematic of the experimental setup. A TM pump with a 2.4-ps pulse width, 1545-nm wavelength, and 10-GHz repetition rate is generated from an actively mode-locked fiber laser (MLFL). A 1-mm-long straight waveguide, with an HR-coated facet (R = 50%) and an AR-coated one, is fabricated on the same chip containing a photonic circuit of a gate switch, as seen in the chip photo in Fig. 1(b). The TM pump pulse is launched into the waveguide from the HR-coated facet on the left. A continuous wave (cw) TE probe at 1560 nm is launched from either the (1) AR- or (2) HR-coated facet for comparison, as shown in Fig. 3(a). Note that the first case (referred to as the reflection configuration) is the same situation as that occurring in the XPM arm of the MI-based gate switch, i.e., the probe is reflected at the facet where the pump is injected. In contrast, the second case (referred to as the transmission configuration) corresponds to the situation where the pump and probe propagate in the same direction. The output probe from the optical circulator is fed into a delay-line-interferometer (DLI) with a 25-ps time delay to convert the phase modulation to intensity modulation. Temporal intensity changes in the probe from the output of the DLI are measured by an optical sampling oscilloscope (OSO) with a time resolution of 0.5 ps. Details of the experimental set-up for XPM measurement are depicted in Fig. 2(a) in ref. 5.

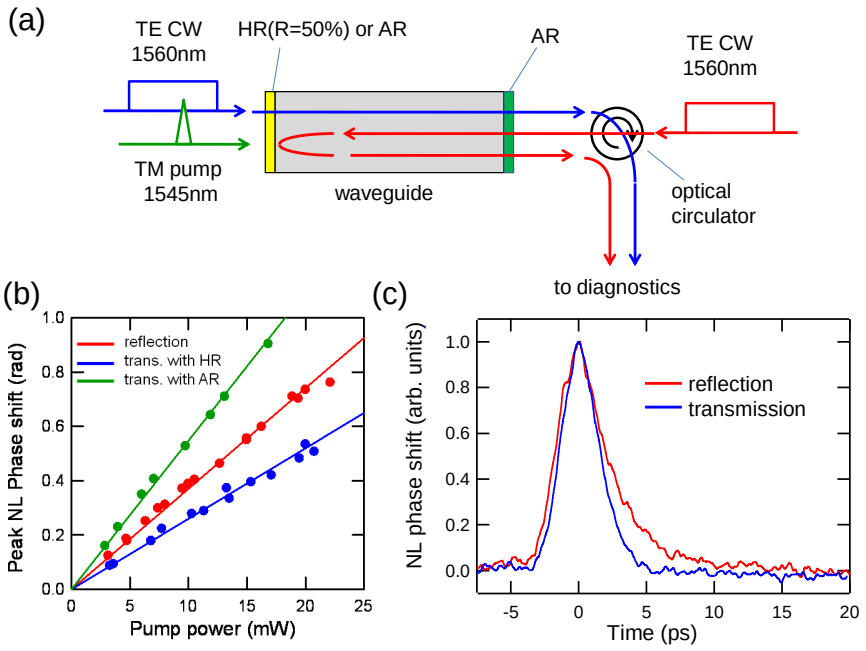

Fig. 3. (a) Schematic diagram of experimental set-up for XPM measurement in a 1-mm-long straight waveguide. In the reflection configuration, the TE-probe cw light is launched from the AR-coated facet on the right, and the probe light reflected at the HR-coated facet is separated from the input light by an optical circulator. In the transmission configuration, the TE probe cw light is launched from the HR- or AR-coated facet on the left. (b) Peak nonlinear phase shift in the probe light at 1545 nm as a function of the average power of the TM pump pulse at 1545

#143905 - $15.00 USD Received 24 Mar 2011; revised 19 May 2011; accepted 1 Jun 2011; published 27 Jun 2011

nm and a 10-GHz repetition rate. XPM efficiency is measured in the following configurations: reflection (0.37 rad/pJ), transmission with HR-coated facet (0.26 rad/pJ), and transmission with AR-coated facet (0.55 rad/pJ). (c) Comparison of temporal changes of nonlinear phase shift in the reflection and transmission configurations.

Figure 3(b) shows the peak nonlinear phase shift as a function of TM pump power for the reflection and transmission configurations. In the transmission configuration, the XPM in a waveguide with both facets AR-coated is also measured. The TM pump power is defined as the power injected into the fiber. For each case, the nonlinear phase shift increases linearly with pump power. The XPM efficiency in the reflection configuration is 0.37 rad/pJ, which is larger than the efficiency of 0.26 rad/pJ in the transmission configuration by a factor of 1.42 under the same pump condition. This is because the probe undergoes XPM twice during co-propagation and counter-propagation in the reflection configuration, whereas it does so only once during co-propagation in the transmission configuration. The maximum increase factor is 2. Previous simulations show that this occurs when ISBT absorption is sufficiently strong, and hence the pump penetration depth (d) is sufficiently short, such that $n_g d/c << \Delta t$ [8], where Δt is the intersubband carrier relaxation time or the pump pulse width and n_g and c are the group index and light velocity, respectively. That is, during counter-propagation, the time necessary for light to pass through the phase-modulated portion in a waveguide is much shorter than Δt. On the other hand, as the current increase factor is less than 2, the light propagation time in the phase-modulated portion is substantially longer than Δt. This causes broadening of the nonlinear response during counter-propagation, which is experimentally confirmed by measuring the temporal response of the nonlinear phase shift in the two cases shown in Fig. 3(c). In the reflection configuration, the decay becomes slow and the tail portion increases, as seen in the waveform of the nonlinear phase shift compared to that in the transmission configuration. However, this slow component is still negligibly small for signal processing at a 160-Gb/s data rate, as will be shown later.

3.2 Characterization of monolithically integrated all-optical gate switch

Figure 4 shows the fiber-to-fiber transmittance between the signal input and signal output ports as a function of the voltage applied to the heater for phase bias control in the gate-switch device. The TE cw light at 1560 nm is launched as an input signal. When the VOA heater voltage is not applied, the extinction ratio, i.e., the loss difference between the constructive and destructive interference conditions, is 36 dB, indicating that the imbalance in light power between the two MI arms due to MZI loss in the VOA is sufficiently small. The loss in the constructive interference condition is −12.4 dB. With increasing VOA voltage, the extinction ratio decreases gradually; interference disappears at 4.2 V, confirming that the reflected power from the VOA arms is completely attenuated at this voltage.

#143905 - $15.00 USD Received 24 Mar 2011; revised 19 May 2011; accepted 1 Jun 2011; published 27 Jun 2011

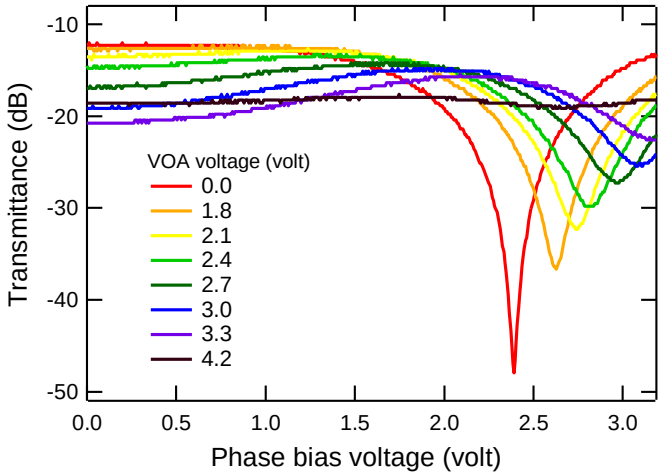

Fig. 4. Fiber-to-fiber transmittance between signal input and signal output ports in a static interference condition as a function of phase bias control voltage for the MI. Measurement is performed at different VOA applied voltage condition. A TE cw light at 1560 nm is launched as the signal.

The gate-switching operation at a 10-GHz repetition rate is examined. A TM pump with a 2.4-ps pulse width, 1545-nm wavelength, and 10-GHz repetition rate is launched from the pump input port, while the TE cw probe at 1560 nm is launched from the signal input port. The temporal changes in the probe signal intensity directed to the output port and returned to the input port are measured by the OSO. The probe signal returned to the input port is separated from the input probe signal by an optical circulator. The phase bias voltage is adjusted so that the signal output port is in the destructive interference condition during no pump injection while the signal input port is in the constructive interference condition. Figure 5(a) shows the temporal changes in signal intensity for each port for a pump pulse energy of 8.6 pJ. A nonlinear phase shift of ~π radians is confirmed from the waveform in the signal returned to the input port in the upper panel of Fig. 5(a), as the probe signal intensity decreases to almost zero upon the injection pump pulse. The XPM efficiency estimated from this result is consistent with the experimental result obtained in the straight waveguide in Fig. 3(b). On the other hand, a gated signal comes out from the signal output port as seen in the lower panel of Fig. 5 (a). This waveform corresponds to the gate-switching window when the present device is operated at a nonlinear phase shift of π radians. The full width at half maximum of the gating window is 4.5 ps.

We examined the gate width as a function of the pump pulse energy, as shown in Fig. 5(b). The pump wavelength is fixed at 1545 nm, whereas the gate width is measured at probe wavelengths of 1535 and 1560 nm. The gate width at both wavelengths increases with pump pulse energy. This increase can be understood considering that the gate-opening efficiency is proportional to the transfer function of $\sin^2(\theta(t)/2)$, where $\theta(t)$ is the nonlinear phase shift occurring in the XPM arms. In gate switching at 1535 nm, gate width increases more rapidly than at 1560 nm. This is because resonant enhancement of the XPM effect in interband dispersion is greater at shorter wavelengths. In fact, it is confirmed that the XPM efficiency at 1535 nm increases from 0.36 rad/pJ at 1560 nm to 0.46 rad/pJ at 1535 nm.

#143905 - $15.00 USD Received 24 Mar 2011; revised 19 May 2011; accepted 1 Jun 2011; published 27 Jun 2011

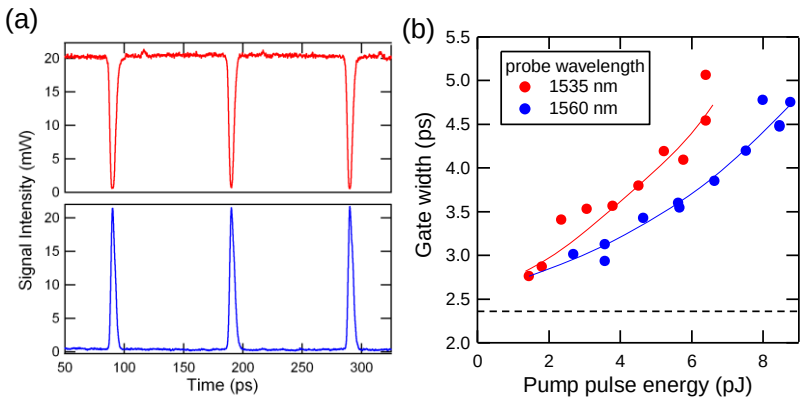

Fig. 5. (a) Gate-switching operation at a 10-GHz repetition rate in which a TM pump of 8.6 pJ/pulse at 1545 nm and a TE probe at 1560 nm are launched. Upper panel: waveform of the probe light intensity returning to the signal input port. Lower panel: waveform of the probe light intensity emerging from the signal output port. (b) Gate width at probe wavelengths of 1535 and 1560 nm as a function of pump pulse energy coupled into the input fiber. The broken horizontal line shows the input pulse width of 2.4 ps as a reference.

Finally, all-optical demultiplexing of a 160-Gb/s signal to a 40-Gb/s signal is demonstrated using the gate-switch device. In this operation, the control pulse opens a gate at a 40-GHz repetion rate to extract a specific 40-Gb/s signal from the 160-Gb/s signals. The experimental set-up is as follows. Two MLFLs with a repetition rate of 10 GHz are used as a control pulse at 1545 nm and a signal pulse at 1560 nm. The 10-GHz optical clock pulse from MLFL1 is data-coded at 10 Gb/s with a pseudo-random bit sequence (PRBS = 2^7-1) using a $LiNbO_3$ intensity modulator. The 10-Gb/s signal is then multiplexed to generate a 40-Gb/s signal using a fiber-based multiplexer that maintains the PRBS sequence. The 40-Gb/s signal is further multiplexed to generate a 160-Gb/s signal pulse (40-Gb/s × 4 channels) by another multiplexer. The 10-GHz pulse from MLFL2 is multiplexed to attain a 40-GHz control light. The 40-GHz TM control and the 160-Gb/s TE signal pulses are launched into the pump input port and signal input ports, respectively. The timing of launching the control pulse is adjusted by an optical-delay line placed outside of the gate switch device.

Figure 6 shows eye diagrams of the 160-Gb/s input signal (upper panel) and the demultiplexed 40-Gb/s signal (lower panel) measured by an OSO. For the demultiplexing experiment, a control pulse energy of 3 pJ is launched into the pump input port. The average optical power injected into the waveguide (120mW) is kept below the damage threshold of ~150 mW. As shown in Fig. 6, the demultiplexed 40-Gb/s signal has an open and clear eye that is fairly identical to the eye diagram of the 160-Gb/s input signal, indicating excellent demultiplexing performance.

#143905 - $15.00 USD Received 24 Mar 2011; revised 19 May 2011; accepted 1 Jun 2011; published 27 Jun 2011

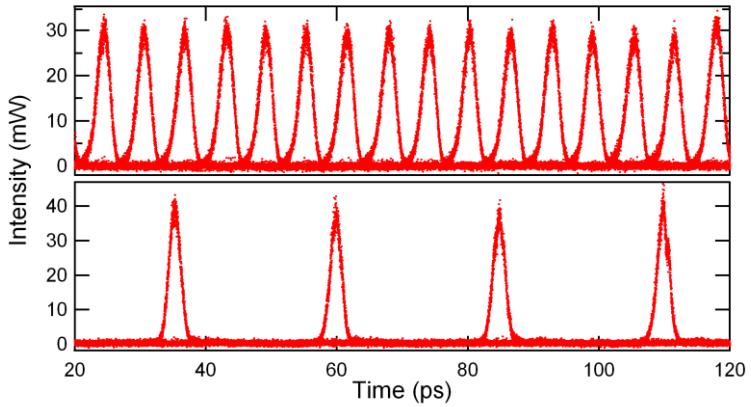

Fig. 6. Eye pattern of the 160-Gb/s input signal (upper panel) and the demultiplexed 40-Gb/s signal (lower panel). A TM control pulse of 3 pJ/pulse at 1545 nm and 40-GHz repetion rate, and a TE signal of 160 Gb/s at 1560 nm are launched.

4. Conclusion

We have developed a compact monolithically integrated all-optical gate switch utilizing optical nonlinearity associated with ISBT in InGaAs/AlGaAs/AlAsSb CDQWs. In this device, an optical nonlinear waveguide using XPM based on ISBT and a MI are monolithically integrated on an InP chip. The MI configuration allows a TM pump light to gain direct access to an MI arm for phase modulation, whereas passive photonic integrated components are designed to work for a TE signal light. The XPM for the TE signal occurs when the signal makes a round trip in a portion of the waveguide where the TM pump is absorbed and causes an index change. We confirmed that the XPM efficiency increases by a factor of 1.42 in the facet reflection configuration used in the present device compared to a single transmission case under the same pump conditions. A performance evaluation of the gate-switching operation showed that full switching of the π-rad nonlinear phase shift for a signal light at 1560 nm is achieved with a pump pulse energy of 8.6 pJ at 1545 nm. All-optical demultiplexing of a 160-Gb/s signal to a 40-Gb/s signal is also demonstrated, in which clear eye opening of the demultiplexed signal is confirmed. The device concept based on an MI configuration and the reflective XPM effect provides a simple means of overcoming the difficulty of connecting active and passive optical waveguides in an integrated all-optical gate switch based on ISBT.

Acknowledgment

This work was partially supported by New Energy and Industrial Technology Development Organization (NEDO).

#143905 - $15.00 USD Received 24 Mar 2011; revised 19 May 2011; accepted 1 Jun 2011; published 27 Jun 2011